The EMBO Journal (2011) 30, 1659–1670 | © 2011 European Molecular Biology Organization | All Rights Reserved 0261-4189/11
www.embojournal.org

THE EMBO JOURNAL

A structural basis for Lowe syndrome caused by mutations in the Rab-binding domain of OCRL1

Xiaomin Hou[1], Nina Hagemann[2], Stefan Schoebel[1], Wulf Blankenfeldt[3], Roger S Goody[1], Kai S Erdmann[2,*] and Aymelt Itzen[1,*]

[1]Department of Physical Biochemistry, Max-Planck-Institute of Molecular Physiology, Dortmund, Germany, [2]Department of Biochemistry II, Ruhr-University Bochum, Bochum, Germany and [3]Department of Biochemistry, University of Bayreuth, Bayreuth, Germany

The oculocerebrorenal syndrome of Lowe (OCRL), also called Lowe syndrome, is characterized by defects of the nervous system, the eye and the kidney. Lowe syndrome is a monogenetic X-linked disease caused by mutations of the inositol-5-phosphatase OCRL1. OCRL1 is a membrane-bound protein recruited to membranes via interaction with a variety of Rab proteins. The structural and kinetic basis of OCRL1 for the recognition of several Rab proteins is unknown. In this study, we report the crystal structure of the Rab-binding domain (RBD) of OCRL1 in complex with Rab8a and the kinetic binding analysis of OCRL1 with several Rab GTPases (Rab1b, Rab5a, Rab6a and Rab8a). In contrast to other effectors that bind their respective Rab predominantly via α-helical structure elements, the Rab-binding interface of OCRL1 consists mainly of the IgG-like β-strand structure of the ASPM-SPD-2-Hydin domain as well as one α-helix. Our results give a deeper structural understanding of disease-causing mutations of OCRL1 affecting Rab binding.

The EMBO Journal (2011) **30,** 1659–1670. doi:10.1038/emboj.2011.60; Published online 4 March 2011
Subject Categories: membranes & transport; molecular biology of disease; structural biology
Keywords: Dent disease; Lowe syndrome; OCRL; Rab; Rab8

Introduction

Membrane trafficking is a fundamental biological process of eukaryotic cells. Vectorial membrane trafficking is crucial for the establishment and maintenance of cell polarity and is strictly regulated by the concerted action of Rab GTPases and phosphatidylinositols (Mellman and Nelson, 2008; Stenmark, 2009). A hallmark of Rab proteins and phosphatidylinositols is their distinct subcellular localization to membrane compartments (Di Paolo and De Camilli, 2006; Stenmark, 2009). For example, Rab5 is mainly localized at early endosomes, whereas Rab6 is localized preferentially at the Golgi apparatus. Likewise, phosphatidylinositol-4,5-bisphosphate is mainly present in the plasma membrane, whereas phosphatidylinositol-4-phosphate is largely confined to the Golgi apparatus. Rab proteins and phosphatidylinositols are both integral parts of the molecular recognition machinery of subcellular membrane compartments, which regulate targeted membrane trafficking between organelles. Rab proteins function as molecular switches by changing from the active GTP-bound to the inactive GDP-bound form and vice versa. Rab GTPases regulate membrane trafficking through the recruitment of effector proteins, such as sorting adaptors, tethering factors, kinases, phosphatases and motors (Segev, 2001; Stenmark, 2009). The Rab-effector proteins specifically interact with the active GTP-bound state of the Rab GTPase. One of these effectors is oculocerebrorenal syndrome of Lowe protein (OCRL1). It shows a broad range of Rab-binding activity and interacts with several Golgi-associated (e.g. Rab1, Rab6 and Rab8) and endosomal (Rab5) Rab proteins (Hyvola *et al*, 2006; Fukuda *et al*, 2008). OCRL1 is a member of the type II family of inositol polyphosphate 5-phosphatases and preferentially dephosphorylates phosphatidylinositol-4,5-bisphosphate ($PI(4,5)P_2$) and phosphatidylinositol-3,4,5-trisphosphate ($PI(3,4,5)P_3$) at the 5-position (Lowe, 2005; Ooms *et al*, 2009). OCRL1 is a peripheral membrane protein mainly localized at the Golgi apparatus and early endosomes (Faucherre *et al*, 2003; Ungewickell *et al*, 2004; Choudhury *et al*, 2005). In addition, growth factor stimulation leads to translocation of OCRL1 to plasma membrane ruffles (Faucherre *et al*, 2003). Mutations of OCRL1 are responsible for the oculocerebrorenal syndrome of Lowe (Lowe syndrome) (Attree *et al*, 1992). Additionally, OCRL1 mutations were recently also identified in a subset of Dent disease patients, which is like Lowe syndrome an X-linked disorder (Hoopes *et al*, 2005). Lowe syndrome is characterized by congenital cataracts, mental retardation and kidney readsorption defects caused by proximal tubule dysfunction (Delleman *et al*, 1977; Kenworthy and Charnas, 1995; Kleta, 2008), whereas Dent disease (type 2) shows a phenotype largely confined to the kidney (Hoopes *et al*, 2005; Utsch *et al*, 2006; Shrimpton *et al*, 2009). OCRL1 has been implicated in several membrane trafficking steps, such as the transport between the early endosome and the Golgi apparatus or endocytosis (Choudhury *et al*, 2005; Erdmann *et al*, 2007). Moreover, recently it was reported that OCRL1 regulates migration and spreading of human dermal fibroblasts (Coon *et al*, 2009). However, the precise function of OCRL1 and its role in disease is not clear.

OCRL1 is a multi-domain protein comprising an N-terminal pleckstrin homology (PH) domain followed by a central inositol-5-phosphatase domain, an ASPM-SPD-2-Hydin (ASH) domain, and a C-terminal, catalytically inactive RhoGAP-like domain (Figure 1) (Erdmann *et al*, 2007; Mao *et al*, 2009). In addition

*Corresponding authors. KS Erdmann, Department of Biochemistry II, Ruhr-Universität Bochum, Universitätsstr. 151, Bochum 44780, Germany. Tel.: +49 234 32 26208; Fax: +49 234 32 14105;
E-mail: kai.erdmann@rub.de or
A Itzen, Department of Physical Biochemistry, Max-Planck-Institute of Molecular Physiology, Otto-Hahn-Str. 11, Dortmund, NRW 44227, Germany.
Tel.: +49 231 133 2305; Fax: +49 231 133 2398;
E-mail: aymelt.itzen@mpi-dortmund.mpg.de

Received: 29 November 2010; accepted: 4 February 2011; published online: 4 March 2011

Figure 1 Schematic representation of the domain architecture of OCRL1.

to binding to multiple Rab proteins, OCRL1 also interacts with clathrin heavy chain, the clathrin adaptor AP2, Rac, Cdc42, the Rab5 effector APPL1 (adaptor protein containing PH domain, PTB domain and leucine zipper motif 1), and the endocytic proteins Ses1/2 (Faucherre *et al*, 2003; Ungewickell *et al*, 2004; Choudhury *et al*, 2005, 2009; Erdmann *et al*, 2007; Swan *et al*, 2010). Interestingly, Lowe syndrome cannot be reproduced in OCRL1-knockout mice, probably because of the existence of the close OCRL1 relative INPP5B. INPP5B has similar domain architecture and substrate specificity, but no clathrin- or AP2-binding sites (Jefferson and Majerus, 1995). In line with at least partially redundant functions of OCRL1 and INPP5B is the fact that OCRL1/INPP5B double-knockout mice are not viable and appear to die early in embryogenesis, whereas OCRL1-knockout mice show no obvious and INPP5B-knockout mice only a minor phenotype (male sterility) (Janne *et al*, 1998).

Recent work by the De Camilli group has given first insights into the detailed molecular structure of OCRL1. The X-ray structure of the ASH-RhoGAP-like tandem domain revealed the localization of the clathrin-binding site within an extended loop in the RhoGAP-like domain. Subsequent NMR-structural analysis of the N-terminus revealed the presence of a PH domain and the presence of a second clathrin-binding site. Together with the previously solved X-ray structure of an inositol-5-phosphatase domain of *Schizosaccharomyces pombe*, a first model for membrane-bound OCRL1 was proposed taking into account recruitment of OCRL1 to the Golgi apparatus and to endosomal membranes via Rab proteins (Erdmann *et al*, 2007; Mao *et al*, 2009). Rab proteins (e.g. Rab1, Rab6, Rab8 and Rab14) may also mediate the localization of OCRL1 to chlamydial inclusions and OCRL1 depletion from host cells impairs chlamydial infection (Moorhead *et al*, 2010). Moreover, active Rab5 and active Rab6 stimulate the 5-phosphatase activity of OCRL1 in hydrolyzing $PI(4,5)P_2$ (Hyvola *et al*, 2006) and several Lowe syndrome causing amino-acid substitutions are localized in the Rab-binding region of OCRL1 (Hichri *et al*, 2010). Thus, investigation of the structural and kinetic basis of the OCRL1–Rab interaction is pivotal for the understanding of the molecular details of OCRL1 function. Here, we present the crystal structure of the Rab-binding domain (RBD) of OCRL1 in complex with active Rab8a (Fukuda *et al*, 2008; Rodriguez-Gabin *et al*, 2010). We have also analysed the kinetics and affinities of OCRL1 binding to the Golgi-associated and endosomal Rab proteins Rab1b, Rab5a, Rab6a and Rab8a. Our results reveal a novel Rab-effector binding mode for OCRL1. In addition, our data contribute valuable information for a structural model of membrane-bound OCRL1. Finally, our results explain the structural effects of disease-causing mutations in OCRL1 leading to a better understanding of Lowe syndrome.

Results and Discussion

Interactions of OCRL1 with Rab proteins

Many Lowe syndrome causing amino-acid substitutions are localized in the 5-phosphatase domain of OCRL1, suggesting that impairment of catalytic activity is part of the OCRL1 disease mechanism (Hichri *et al*, 2010). Major substrates for OCRL1 are the membrane localized phosphatidylinositols ($PI(4,5)P_2$) and ($PI(3,4,5)P_3$). Thus, understanding the precise mechanism of membrane recruitment of OCRL1 is crucial for the understanding of OCRL1 function. Two mechanisms of membrane recruitment have been described for OCRL1. Recruitment to plasma membrane localized membrane ruffles after growth factor stimulation has been attributed to interaction with activated Cdc42, while localization of OCRL1 to the Golgi apparatus and endosomal membranes has been shown to be mediated via Rab proteins (Faucherre *et al*, 2003; Hyvola *et al*, 2006).

The Rab-binding site of OCRL1 was mapped to a region from amino acids 540–725 in a previous report (Hyvola *et al*, 2006) (for a schematic depiction of the domain architecture of OCRL1 see Figure 1). Various data indicate binding of OCRL1 to a number of different Rab proteins *in vitro* (Hyvola *et al*, 2006; Fukuda *et al*, 2008). The interactions were also further supported by co-localization in cells for some OCRL1/Rab pairs; however, the affinities for their interactions have not been determined. Using a fluorescence-based approach, we were able to monitor the binding of $OCRL1_{539-901}$ (OCRL1 amino acids 539–901) to mantGppNHp (a non-hydrolyzable and fluorescent GTP analogue)-loaded Rabs (Rab1b, Rab3a, Rab5a, Rab6a, Rab7, Rab8a, Rab13, Rab14 and Rab31) by exploiting the change in fluorescence polarization (Supplementary Figure S1). The fluorescence polarization increased upon Rab binding to $OCRL1_{539-901}$, indicating complex formation. The reaction was fully reversed by displacement of the mantGppNHp-loaded Rab from $OCRL1_{539-901}$ with an excess of non-fluorescent Rab8a:GppNHp (Supplementary Figure S1). In agreement with previous reports, no complex formation was observed with Rab7 protein (Fukuda *et al*, 2008).

Since the binding specificity of OCRL1 for Rab proteins is rather broad, we were interested whether a certain Rab is preferably bound *in vitro*. Hence, we determined the affinity of various Rab:$OCRL1_{539-901}$ complexes (Rab1b, Rab5a, Rab6a, Rab8a) using equilibrium titrations combined with fluorescence polarization as an indicator of complex formation (Figure 2A). Among the tested Rab proteins, Rab8a:mantGppNHp revealed the highest affinity towards $OCRL1_{539-901}$, with a dissociation equilibrium constant (K_D) of 0.9 μM. Rab1b, Rab5a and Rab6a were bound less strongly with K_D values of about 4 μM (Figure 2A). Thus, Rab8a appears to be the preferred *in vitro* binding partner of OCRL1 among the Rabs tested. Strong interaction of OCRL1 with Rab8a is also supported by significant co-localization of both proteins in Hela cells (Supplementary Figure S2). Previously, the relative affinities to OCRL1 had been reported for Rab8a, Rab6a, Rab5a and Rab1a with Rab8a showing the lowest relative affinity to OCRL1 and Rab6a having the highest (Hyvola *et al*, 2006). Our findings differ from this report, possibly due to the different techniques applied. Thus, we measured binding affinities in solution, while the previous report used surface-immobilized OCRL1 for its binding study. In addition, we used wild-type Rab:mantGppNHp proteins for our interaction studies, whereas the other report applied GST-fusion proteins of constitutively active Rab mutants. Also, an indirect influence of the mant-group at the ribose moiety of mantGppNHp cannot be excluded and might

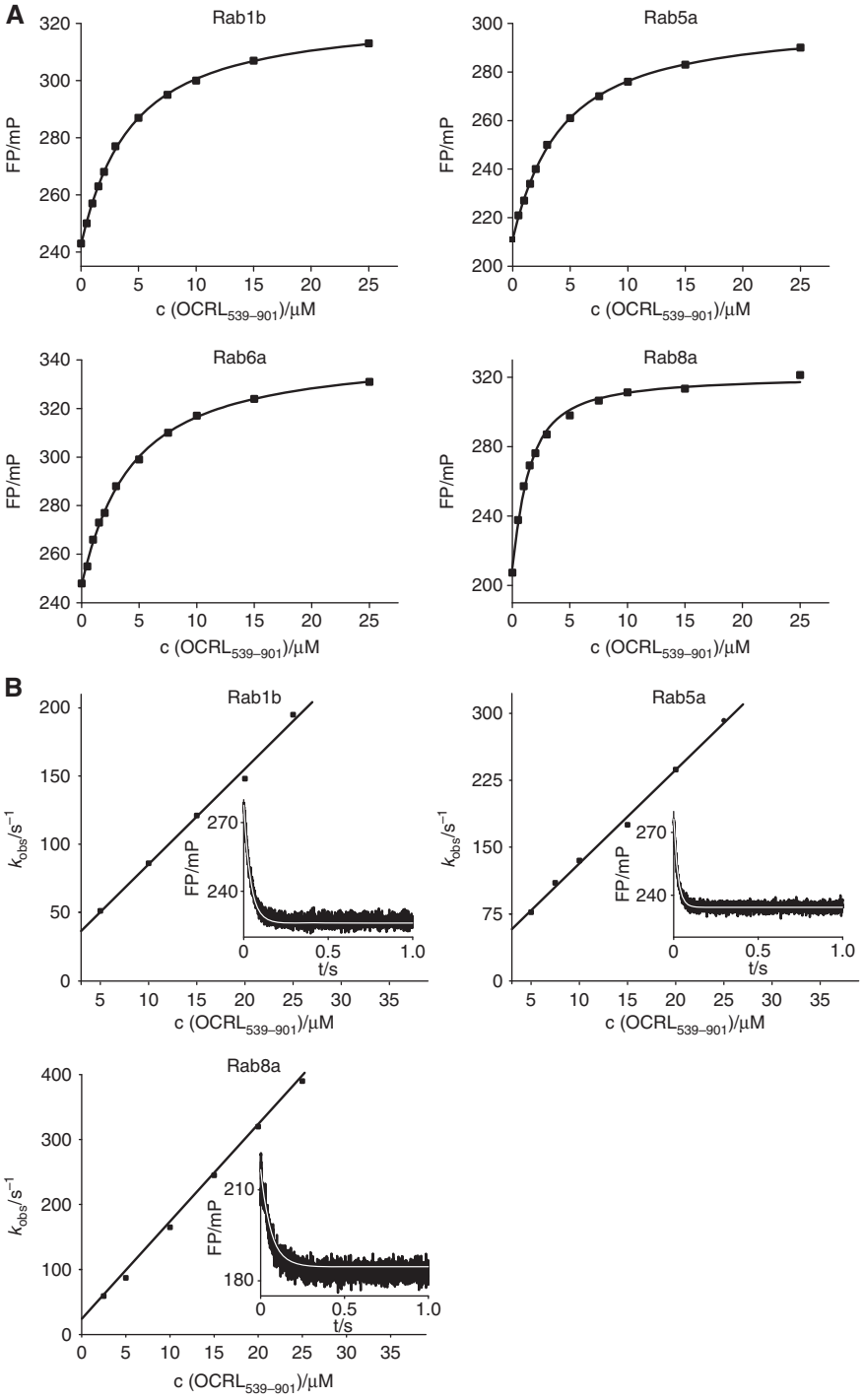

Figure 2 OCRL1 binds different exocytic and endocytic Rab proteins with moderate affinities. (**A**) Fluorescence polarization based equilibrium titration of 1 μM Rab1b:mantGppNHp, Rab5a:mantGppNHp, Rab6a:mantGppNHp or Rab8a:mantGppNHp with $OCRL1_{539–901}$, respectively. (**B**) Association and dissociation kinetics of Rab1b:mantGppNHP, Rab5a:mantGppNHp and Rab8a:mantGppNHp with $OCRL1_{539–901}$, respectively, monitored by the change in fluorescence polarization using stopped-flow apparatus (c(RabX:mantGppNHp) = 1 μM). The individual observed association rate constants are linearly dependent on the $OCRL1_{539–901}$ concentration and were fitted to a straight line, yielding the association rate constant. (Insets) The dissociation of fluorescent RabX:mantGppNHp (2 μM) from its complex with $OCRL1_{539–901}$ was monitored by displacement with a 10-fold molar excess of non-fluorescent Rab using the stopped-flow apparatus. The time-dependent decrease in fluorescence polarization, indicative of complex dissociation, was fitted to a single exponential function (white line) to determine the dissociation rate constants. FP, fluorescence polarization; mP, milli-polarization units.

have a minor effect on the binding of the derivatized Rab protein to OCRL1. The K_D values obtained in the described equilibrium titrations in the present study were confirmed by the kinetic investigations described in the next section.

Using these Rab:mantGppNHp complexes, we also investigated the dynamics of Rab:$OCRL1_{539–901}$ complexes by determining their association and dissociation rate constants (k_{on} and k_{off}, respectively). The association process was

Table I Summary of equilibrium constants (K_D) of Rab proteins[a]

	K_D (equilibrium titration)/μM	K_D (from kinetics)/μM
Rab1b	3.7	3.7
Rab5a	3.6	3.8
Rab6a	3.7	N/A
Rab8a	0.9	1.1

N/A, not assessed.
[a]$OCRL1_{539–901}$ was used to determine the kinetics.

monitored by the time-dependent change in fluorescence polarization in a stopped-flow apparatus. Single exponential fitting of individual traces yielded the observed pseudo first-order rate constant of the association reaction at a specific $OCRL1_{539–901}$ concentration. Plotting the observed rate constants (k_{obs}) against the $OCRL1_{539–901}$ concentration gave a straight line, with the slope equal to the association rate constant (k_{on}) for each Rab protein (Rab1b: $k_{on} = 7.0 \times 10^6\,M^{-1}\,s^{-1}$; Rab5a: $k_{on} = 1.05 \times 10^7\,M^{-1}\,s^{-1}$; Rab8a: $k_{on} = 1.5 \times 10^7\,M^{-1}\,s^{-1}$) (Figure 2B). The dissociation rate constants (k_{off}) were determined by displacing the fluorescent Rabs from their complex with $OCRL1_{539–901}$ with a 10-fold molar excess of non-fluorescent Rab:GppNHp (Rab1b: $k_{off} = 25\,s^{-1}$ Rab5a: $k_{off} = 40.1\,s^{-1}$; Rab8a: $k_{off} = 16.2\,s^{-1}$) (Figure 2B). From the association and dissociation rate constants, K_D values for the affinity of the Rab:mantGppNHp–$OCRL1_{539–901}$ interaction (Rab1b: $K_D = 3.7\,\mu M$; Rab5a: $K_D = 3.8\,\mu M$; Rab8a: $K_D = 1.1\,\mu M$) could be calculated. As shown in Table I and Figure 2, Rab8a:mantGppNHp displays the highest affinity toward $OCRL1_{539–901}$, while the other evaluated Rabs are bound about four-fold more weakly.

Previous reports suggested that Rab proteins bind to OCRL1 within the linker region between the 5-phosphatase and RhoGAP-like domains (Figure 1). To further localize the Rab-binding site, we produced various N-terminal and C-terminal truncations of OCRL1 and analysed the binding to Rab8a:GppNHp by analytical gel filtration (Supplementary Figure S3). The constructs $OCRL1_{540–678}$ and $OCRL1_{555–678}$ were able to bind Rab8a:GppNHp, but the $OCRL1_{560–678}$ fragment failed to interact with active Rab8a. The construct $OCRL1_{555–668}$ could not bind to Rab8a:GppNHp since the protein was prone to aggregation, indicating an unfolded ASH domain. Hence, $OCRL1_{555–678}$ represents the minimal Rab-binding construct.

Crystal structure of the $Rab8a_{6–176}$:GppNHp: $OCRL1_{540–678}$ complex

In order to understand the molecular basis of the interaction between Rab proteins and OCRL1, we determined the crystal structure of a complex between active, GppNHp-loaded Rab8a (amino acids 6–176, $Rab8a_{6–176}$) and OCRL1 (amino acids 540–678, $OCRL1_{540–678}$) at 2.0 Å resolution. The crystal structure contains four individual complexes per asymmetric unit (for data collection and refinement statistics, see Table II). Some residues in the N-terminal regions of two $OCRL1_{540–678}$ molecules (residues 540–548 of chain B and D) were not visible in electron density, and thus were omitted from the final model. Since the mode of interaction among the four complexes in the asymmetric unit is highly similar (excluding small differences due to crystal packing) (Supplementary Figure S4), we discuss only one representative complex structure here.

Table II Data collection and refinement statistics for $Rab8a_{6–176}$:$OCRL1_{540–678}$

Data collection[a]	
Space group	C2
Cell dimensions	
A, *B*, *C* (Å)	157.15, 55.34, 173.84
α, β, γ (deg)	90.00, 91.93, 90.00
Resolutions (Å)	20–2.0 (2.1–2.0)
R_{merge} (%)[b]	5.5 (33.4)
$I/\sigma(I)$	15.4 (4.2)
Completeness (%)	98.3 (97.0)
Redundancy	3.2 (3.0)
Refinement	
No. of reflections	320 388 (39 313)
R_{work}/R_{free}	20.9/24.1
No. of atoms	
Protein	9954
Ligand/ion	142
Water	324
B-factors	
Protein	38
Ligand/ion	28
Water	39
R.m.s. deviation	
Bond lengths (Å)	0.014
Bond angles (deg)	1.412

Values in parentheses refer to the highest resolution shell.
[a]The data set was collected from one single crystal on beamline X10SA of the Swiss Light Source (Paul Scherrer Institute, Villigen, Switzerland).
[b]Calculated as defined by Diederichs and Karplus.

A cartoon representation of the $Rab8a_{6–176}$:$OCRL1_{540–678}$ complex is shown in Figure 3A. In the complex, $Rab8a_{6–176}$ adopts the common GTPase fold, which consists of six central β-strands ($\beta1_R$–$\beta6_R$) surrounded by five α-helices ($\alpha1_R$–$\alpha5_R$) (subscripts 'R' and 'O' denote elements of Rab8a and OCRL1, respectively). $OCRL1_{540–678}$ consists of the ASH domain and an elongated helix ($\alpha1_O$ in green) belonging to the 5-phosphatase domain. The ASH domain of $OCRL1_{540–678}$ forms two layers of β-sheets fold and is closely related to the members of the family of immunoglobulin-like β-sandwiches (Erdmann *et al*, 2007).

The Rab8a:OCRL1 complex interface

Complex formation leads to the burying of 1733 $Å^2$ of solvent-accessible surface area. The majority of contacts in the complex are mediated by the $\alpha1_O$-helix and the β-strand 9 ($\beta9_O$) of OCRL1, and Switch I, Switch II and the Interswitch region of Rab8a (Figure 3A).

The complex crystal structure reveals a Rab-binding site in $OCRL1_{540–678}$ that consists of two separate elements: The first site of protein–protein contact (binding site I) in OCRL1 is located in the linker region between the ASH domain and 5-phosphatase domain. The interactions between Rab8a and OCRL1 in binding site I are mostly of polar nature (Figure 3B). The amino acids $D555_O$ to $N559_O$ in the N-terminal region of OCRL1 are essential for binding Rab proteins (Supplementary Figure S3). $D555_O$ and $R556_O$ form side chain interactions with $T49_R$ in the Interswitch region and $E30_R$ in Switch I, respectively. In addition, the adjacent residue $N559_O$ binds strongly with the main chain of $I47_R$ in the Interswitch region via a hydrogen bond. Hence, the

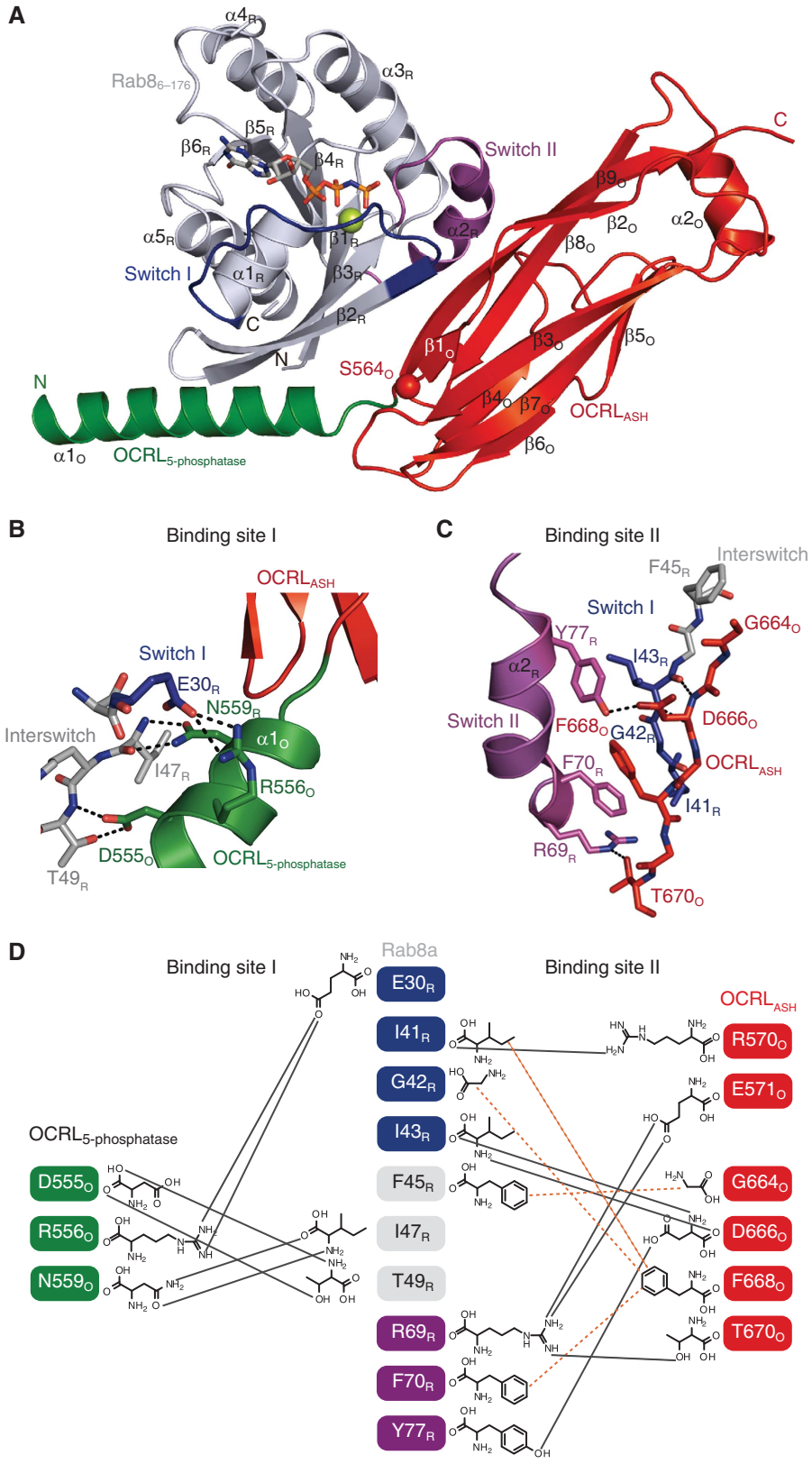

Figure 3 Crystal structure of the Rab8a$_{6–176}$:OCRL1$_{540–678}$ complex (**A**) Cartoon representation of the Rab8a$_{6–176}$:OCRL1$_{540–678}$ complex. Rab8a$_{6–176}$ is shown in grey, with Switch I in blue and Switch II in magenta. OCRL1$_{540–670}$ is in green (helix α1$_O$ of the 5-phosphatase domain) and red (ASH domain). The position of S564$_O$ (S564P$_O$ causes Lowe syndrome) is indicated with a red sphere. (N, N-termini; C, C-termini; sticks, non-hydrolyzable GTP-analogue GppNHp; green sphere, Mg^{2+}, colouring is kept consistent throughout all panels). (**B**, **C**) Detailed view of interactions between Rab8a$_{6–176}$ with α1$_O$-helix (binding site I, (**B**)) and the ASH domain (binding site II, (**C**)) of OCRL1$_{540–678}$. The Switch I region of Rab8a and the β9$_O$-strand of OCRL1 are in stick representation to show the main-chain interactions (black dashes: polar interactions). (**D**) Schematic view of Rab8a–OCRL1 interactions (black lines: hydrogen bonds, brown dashes: hydrophobic contacts).

significance of the amino acids 555–559 of OCRL1 for Rab binding (Supplementary Figure S3) is apparent from the structure of the complex interface.

All known structurally characterized Rab-effector proteins bind to their respective Rab proteins mainly via 1–2 α-helices (Zhu *et al*, 2004; Eathiraj *et al*, 2005, 2006; Kawasaki *et al*, 2005; Wu *et al*, 2005; Jagoe *et al*, 2006; Chavas *et al*, 2008; Kukimoto-Niino *et al*, 2008). In contrast to these established binding modes, OCRL1 Rab8a interacts with the Rab-binding motif of OCRL1 via a β-strand ($\beta9_O$), which forms the Rab-binding site II. The interaction between Rab8a and OCRL1 in binding site II is mediated by both hydrophobic and polar contacts. The side chain of $F668_O$ in OCRL1 penetrates into a hydrophobic core of Rab8a, which is formed by $I41_R$ and $G42_R$ in the Switch I region and $F70_R$ in the Switch II region. Moreover, $G664_O$ of OCRL1 Interacts with $F45_R$ in the Rab8a Interswitch region. Besides these hydrophobic interaction, $D666_O$ forms hydrogen bonds with the main chain of $I43_R$ of Switch I and the hydroxyl oxygen of $Y77_R$ of Switch II. An additional polar interaction is seen between $T670_O$ and $R69_R$ of the Rab8a Switch II region. Furthermore, $R570_O$ and $E571_O$ from the N-terminal region of the ASH domain interact with the main chain of $I42_R$ and side chain of $R69_R$, respectively (Figure 3C and D).

The molecular interactions seen in the Rab8a:OCRL1 complex also provide a structural understanding of previous Rab-binding studies (D555E, S568G, S564P, G664D, N606K; Supplementary Figure S5) (Hyvola *et al*, 2006). According to the complex structure, D555 and G664 are responsible for the interaction with the Interswitch region by forming polar and hydrophobic interactions, respectively. Consequently, the D555E and G664D substitutions generated by Hyvola *et al* (2006) reduced the Rab-binding activity of OCRL1 *in vitro* and impaired OCRL1 membrane localization *in vivo*, hence supporting their implication in Rab8a–OCRL1 complex formation. The amino acids S568 and N606 are not involved in establishing the complex interface and their substitutions (S568G and N606K) do not influence Rab binding or OCRL1 membrane recruitment (Hyvola *et al*, 2006). Variant S564P had the strongest effect on Rab binding, abolishing it completely (Hyvola *et al*, 2006). Based on our complex structure, the substitution S564P is expected to destabilize the conformation of binding site II, since this residue appears to be an integral part of the beginning of the ASH domain, leading to complete loss of Rab-binding activity. Additionally, the S564P mutation could impair the correct relative arrangement of the α1-helix and the ASH domain, since proline has reduced conformational freedom compared with serine. Since S564 is at the C-terminal end of the α1-ASH linker region, its mutation to proline possibly affects Rab binding by impairing the orientation of helix α1 (Rab-binding site I) and the ASH domain (Rab-binding site II). Thus, the *in vivo* and *in vitro* effects of OCRL1 point mutations reported previously perfectly correlate with their relevance for Rab8a:OCRL1 complex formation as suggested by the complex crystal structure.

The Rab8a:OCRL1 interaction mode in comparison to other Rab effectors

In the active state, Rab proteins recruit diverse effectors to specific subcellular compartments. A number of Rab-effector crystal structures have been reported. These are (1) Rab3:Rabphilin, Rab27a:Slp2a and Rab27b:Slac2-a, which are associated with secretory vesicles (Ostermeier and Brunger, 1999; Chavas *et al*, 2008; Kukimoto-Niino *et al*, 2008); (2) Rab7:RILP (Rab7-interacting lysosomal protein), which is involved in regulating fusion between lysosomes and endosomes (Wu *et al*, 2005); (3) Rab4:Rabenosyn-5, Rab22:Rabenosyn-5 and Rab5:EEA1 (early endosomal autoantigen 1), which coordinate endosomal traffic (Eathiraj *et al*, 2005; Mishra *et al*, 2010); (4) Rab5:Rabaptin5, which is implicated in early endosome fusion (Zhu *et al*, 2004); (5) Rab11:FIP2 (Rab11-family interacting protein 2) and Rab11:FIP3, which are involved in regulating endocytic recycling (Eathiraj *et al*, 2006; Jagoe *et al*, 2006); (6) Rab6:Rab6IP1 (Rab6-interacting protein 1); and (7) Rab6:GCC185, which regulate endosome to Golgi transport (Burguete *et al*, 2008; Recacha *et al*, 2009). In all of the previously reported structures of Rab-effector complexes, the RBD is exclusively formed by an α-helical region in the effector (Lee *et al*, 2009). In contrast to these helix-dominated RBDs, OCRL1 interacts with Rab8a not only via an α-helix ($\alpha1_O$) but also via β-strand $\beta9_O$ from the all-β ASH domain in binding site II. The general binding interfaces of Rabs include the Switch and Interswitch regions and are either centred on or overlap with an invariant hydrophobic triad ($F45_R$ and $W62_R$ in the Interswitch and $Y77_R$ in Switch II according to the sequence of Rab8a) (Merithew *et al*, 2001; Lee *et al*, 2009). However, in the $Rab8a_{6-176}$:$OCRL1_{540-678}$ complex, not all of the three aromatic residues of the hydrophobic core participate in the binding interface. $W62_R$ in the Interswitch region is not involved in OCRL1 binding, while $Y77_R$ in the Switch II region associates with $D666_O$ only via a hydrogen bond interaction, but not a hydrophobic interaction as in other Rab-effector complexes. Only $F45_R$ in the Interswitch region interacts with $G664_O$ in OCRL1.

When comparing the OCRL1/Rab-binding mode with that of other Rab effectors, it seems that the invariant hydrophobic triad may not be such a critical requirement for the Rab binding of OCRL1 as for other Rab-effector interactions (reviewed in Lee *et al*, 2009; Itzen and Goody, 2011). Although there are numerous effectors that can bind to several different Rab proteins, an effector binding as broad as observed for OCRL1, which includes Rab proteins from completely different subfamilies, is unusual. Based on previous interaction studies, different Rab proteins bind to the same site in OCRL1, although with subtle differences (Hyvola *et al*, 2006). It is therefore appropriate to consider why OCRL1 binds to such a broad variety of different Rab proteins. It has been suggested that the hydrophobic triad of Rab proteins represents a main determinant for Rab subfamily specific effector binding (Merithew *et al*, 2001). The side chain conformations of this conserved hydrophobic triad ($F45_R$, $W62_R$ and $Y77_R$) in the active state are similar for members of a Rab subfamily but different among subfamilies, and this structural plasticity is suggested to be an important determinant for Rab-effector specificity (Merithew *et al*, 2001; Grosshans *et al*, 2006). In the case of the Rab–OCRL1 interaction, the hydrophobic triad appears to have only a minor role in OCRL1 binding, since the central $W62_R$ residue in Rab8a is not involved in any interactions with residues of OCRL1. Thus, the minor involvement of the hydrophobic triad of Rabs in OCRL1 binding might serve as an explanation for the low Rab-binding specificity of OCRL1. It will be interesting to see whether effectors with a wide Rab-binding

range comparable to OCRL1 (Fukuda *et al*, 2008) employ a similar structural mechanism, that is by omitting the hydrophobic triad of Rabs as a main binding determinant to achieve interaction with multiple Rabs.

The broad Rab-binding specificity of OCRL1 contributes to its diverse subcellular localization. siRNA experiments have demonstrated that knockdown of Rab1 together with Rab6 leads to a significantly reduced binding of OCRL1 to the Golgi apparatus. It was also demonstrated that constitutively expressed Rab5 can translocate OCRL1 from the cytosol to enlarged endosomes. Point mutations abolishing binding to Rab proteins lead to complete delocalization of OCRL1 to the cytosol (Hyvola *et al*, 2006). However, other targeting mechanisms might exist, for example transient localization of OCRL1 to late clathrin-coated pits has been demonstrated to rely on its two clathrin-binding motifs (Mao *et al*, 2009).

APPL1/Ses1 peptides do not influence the Rab8a:OCRL1 interaction

The ASH domain is not only required for binding to Rab proteins but also for binding to the Rab5-effector protein APPL1 (Erdmann *et al*, 2007), as well as to the two novel endocytic proteins Ses1/2 (Swan *et al*, 2010). APPL1/Ses interactions with OCRL1 are both mediated by a conserved short amino-acid motif (Phe and His [F&H] motif) in APPL1/Ses1. We asked whether binding of APPL1 and Ses1 modulates the affinity of OCRL1 for Rab proteins. To do this, we determined the affinity of Rab8a:mantGppNHp to $OCRL1_{539–901}$ by equilibrium titration as described above in the presence of the APPL1 and Ses1 OCRL1 binding peptides (SFQQRHESLRP and PFARLHECYGQEI, respectively) (Swan *et al*, 2010) (Figure 4). The concentrations used are orders of magnitude higher than the known K_D values for the peptides for OCRL1, ensuring binding under these conditions. The binding activity of the synthesized peptides to $OCRL1_{539–901}$ has been independently confirmed by isothermal titration calorimetry, yielding results that are comparable to the ones reported by Swan *et al* (2010). The K_D of the complex between Rab8a:mantGppNHp and $OCRL1_{539–901}$ was unchanged by the presence of APPL1 or Ses1 peptides, suggesting they have no modulatory effect on the stability of the Rab8a:OCRL1 complex (Figure 4). Apparently, the interaction of Rab with OCRL1 is independent of the simultaneous binding of the APPL1 or Ses1 peptides to OCRL1, indicating no communication of the APPL1/Ses1-binding site with the Rab-binding site.

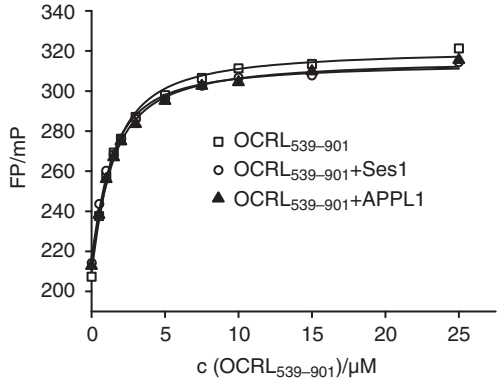

Figure 4 The binding of APPL1 and Ses1 peptides does not alter the dissociation equilibrium constant of the Rab8:mantGppNHp–$OCRL1_{539–901}$ interaction. The experimental setup described in Figure 2A was repeated in the presence of 200 μM APPL1 peptide or 100 μM Ses1 peptide with 1 μM Rab8a:mantGppNHp and varying concentrations of $OCRL1_{539–901}$ (FP, fluorescence polarization; mP, milli-polarization units).

A structural basis for Lowe syndrome

Two missense mutations causing Lowe syndrome are responsible for amino-acid substitutions in the minimal Rab-binding region of OCRL1 (L634P and F668V). Substitution L634P is likely to destabilize the ASH domain fold, which is in line with complete loss of binding to APPL1 and Ses proteins. However, F668V retained the binding to APPL1 and Ses1/2, making an APPL1/Ses1 interaction deficiency unlikely to account for disease development. Thus, the molecular basis for this disease-causing mutation remained unclear (Swan *et al*, 2010). In the $Rab8a_{6–176}$:$OCRL1_{540–678}$ structure, F668 participates in the complex interface by establishing a multitude of contacts within a hydrophobic groove of Rab8a (Figure 5A and B). We speculated that the F668V substitution impairs the interaction with Rab8a due to the lower hydrophobicity of valine compared with phenylalanine. Furthermore, this effect should be even more pronounced with an F668A substitution in OCRL1. This hypothesis was confirmed by determining the dissociation constants between active Rab8a:mantGppNHp and the $OCRL1_{539–901}$ variants (F668V or F668A) by equilibrium titration (Figure 5C). The affinity of $OCRL1_{539–901}$ F668V was decreased 5.8-fold compared with the wild-type protein ($K_{D,Rab8:OCRL1} = 0.9\,\mu M$, $K_{D,Rab8:OCRL1\ F668V} = 5.2\,\mu M$). The affinity of the F668A variant was decreased by a factor of 6.7 compared with the wild-type protein ($K_{D,Rab8:OCRL1\ F668A} = 6.0\,\mu M$). Thus, the variants F668V and F668A of OCRL1 weaken the binding towards active Rab8a. In addition, the amino-acid substitutions F668V and F668A also significantly impair the binding to Rab1b, Rab5a and Rab6a (Supplementary Figure S6). To confirm weakened binding of OCRL1 (F668V) to Rab8a by an independent assay, we performed pull-down experiments using GST-fusion proteins of $OCRL1_{539–901}$ and $OCRL1_{539–901}$ F668V. Using this assay, binding of Rab8a to $OCRL1_{539–901}$ was detected; however, no binding could be detected between Rab8a and $OCRL1_{539–901}$ F668V. In contrast, both OCRL1 constructs bound APPL1 efficiently, indicating selective impairment of binding to Rab8a for $OCRL1_{539–901}$ F668V (Figure 5D). It has been previously shown that interaction with Rab proteins is crucial for OCRL1 membrane recruitment. Thus, we tested whether the Lowe syndrome mutation F668V changes the subcellular localization of OCRL1. Transfection of GFP–OCRL1 F668V into Hela cells revealed that the mutation leads to a large increase in cytosolic localization of OCRL1 and to a significant reduction at the Golgi apparatus and vesicular structures (Figure 5E). Co-transfection experiments of Myc-tagged wild-type OCRL1 together with GFP–OCRL1 F668V also demonstrated significant localization differences between mutant and wild-type OCRL1 for example reduced localization at subcellular membranes and a higher cytosolic pool for mutant OCRL1 (Figure 5F). The observed differences in binding affinity and subcellular localization are completely in line with our predictions based on the Rab8a:OCRL1 complex structure.

In summary, the point mutation F668V is so far the only Lowe syndrome causing variant, which selectively affects the Rab-binding properties of OCRL1, giving direct *in vivo* evidence for the importance of Rab interaction for OCRL1 function(s).

Structural model of the interaction of OCRL1 and Rab8a at the membrane interface

The $Rab8a_{6-176}$:$OCRL1_{540-678}$ complex structure allows us to expand the previous structural model of OCRL1 at the membrane interface (Erdmann *et al*, 2007) (Figure 6):

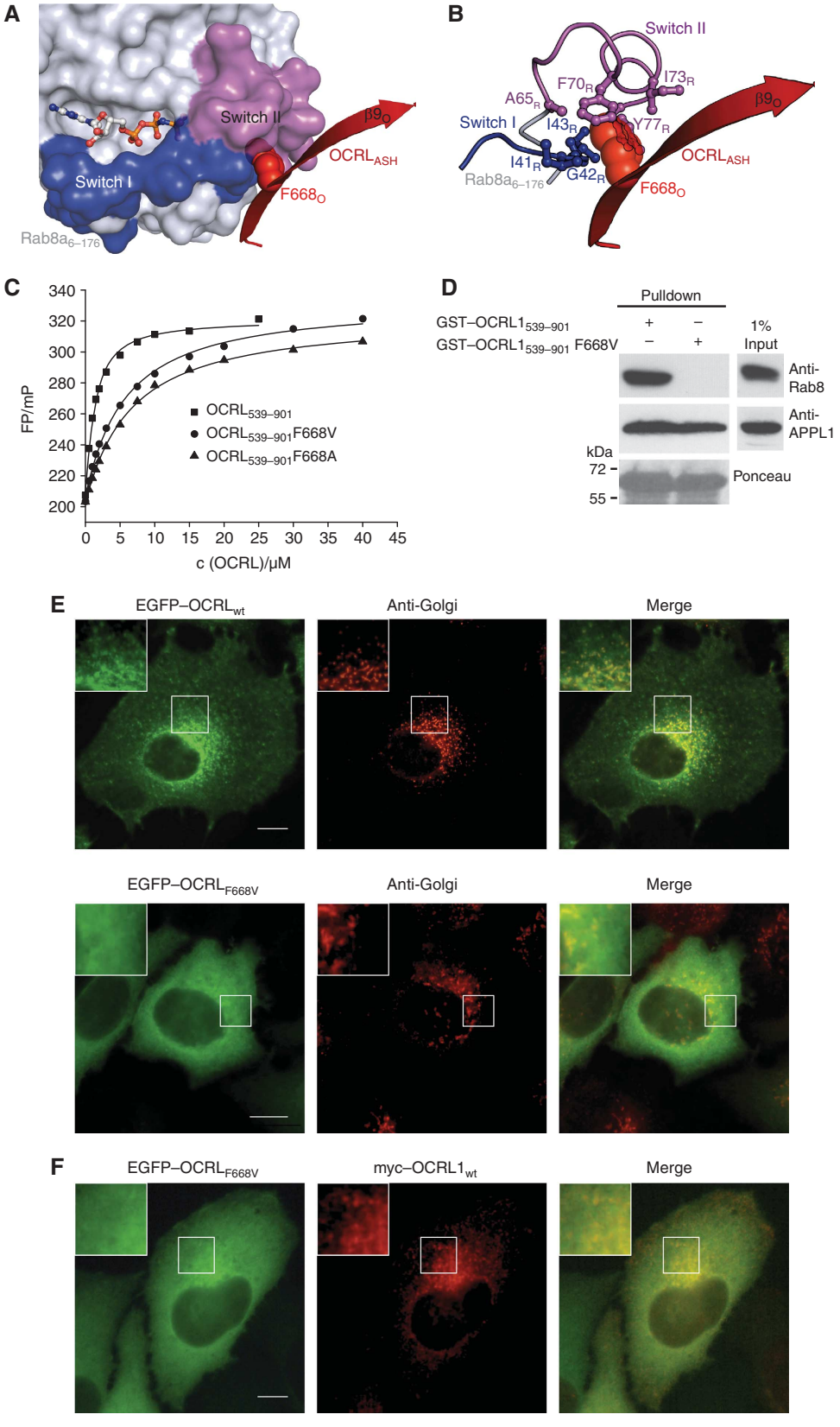

Superimposition of the C-terminal α-helix of the inositol polyphosphate 5-phosphatase domain of the yeast homolog of synaptojanin (Tsujishita *et al*, 2001) with the helix $\alpha1_O$ of OCRL1 from our complex structure together with a superimposition of the ASH domain of the ASH-RhoGAP (Erdmann *et al*, 2007) structure yields an approximate model of OCRL1. The possible relative orientation of this virtual construct towards a membrane is obtained from the position of inositol-1,4-bisphosphate bound to the inositol polyphosphate 5-phosphatase domain in the X-ray structure of the synaptojanin yeast homolog (Tsujishita *et al*, 2001). In this model, Rab8a is centrally located between the inositol polyphosphate 5-phosphatase and the RhoGAP domain. The nucleotide-binding pocket of Rab8a is pointing away from the membrane and faces the cytosol, whereas the structurally flexible C-terminus of the GTPase is oriented towards the lipid bilayer, thereby leading to undisturbed interaction of the single C-terminal geranylgeranyl moiety of Rab8a (Joberty *et al*, 1993) with the membrane. Since Switch I and Switch II are oriented towards the cytosol in our model, an interaction with additional Rab regulators and/or effectors is in principle possible, which could further modulate the Rab–OCRL1 interaction.

In this study, we have presented the first structure of the RBD of OCRL1 in complex with a Rab protein (Rab8a). Based on our results we have rationalized the structural consequences of known Lowe syndrome causing mutations leading to substitutions in the RBD. However, the identification of Lowe syndrome mutations is still ongoing, and recently 51 novel mutations were reported (Hichri *et al*, 2010). Our results will help to understand the functional consequences of newly identified mutations in the future. Finally, our data extend the current structural understanding of OCRL1 and support the idea that impairment of Rab binding contributes to the complex disease mechanism in Lowe syndrome.

Materials and methods

Protein expression and purification

Human Rab8a and OCRL1 genes were synthesized as codon-optimized DNA for expression in *Escherichia coli* (MR GENE, Regensburg, Germany). The truncated $Rab8a_{6–176}$ was subcloned into a modified pET19 vector that contained an N-terminal hexahistidine (His_6) tag and a Tobacco Etch Virus (TEV) protease cleavage sequence. The expression and purification of $Rab8a_{6–176}$ were performed as described for full-length Rab8a (Bleimling *et al*, 2009). $OCRL1_{539–901}$ was cloned into a modified pMAL vector containing an N-terminal His_6-maltose binding protein (MBP)-tag and TEV protease cleavage sequence. $OCRL1_{540–678}$, $OCRL1_{555–678}$, $OCRL1_{560–678}$ and $OCRL1_{555–668}$ were cloned by the Dortmund Protein Facility (http://www.mpi-dortmund.mpg.de/misc/dpf/) into a pOPINM-vector (N-terminal His_6-MBP tag followed by a PreScission protease cleavage sequence) by the in-fusion cloning method (Berrow *et al*, 2007). OCRL1 constructs were expressed in *Escherichia coli* BL21 (DE3) overnight at 20°C after induction with 0.2 mM isopropyl-β-dithiogalactopyranoside (IPTG). Proteins were purified from bacterial lysate using nickel-nitrilotriacetic acid (Ni-NTA) column pre-equilibrated with buffer A (50 mM HEPES,

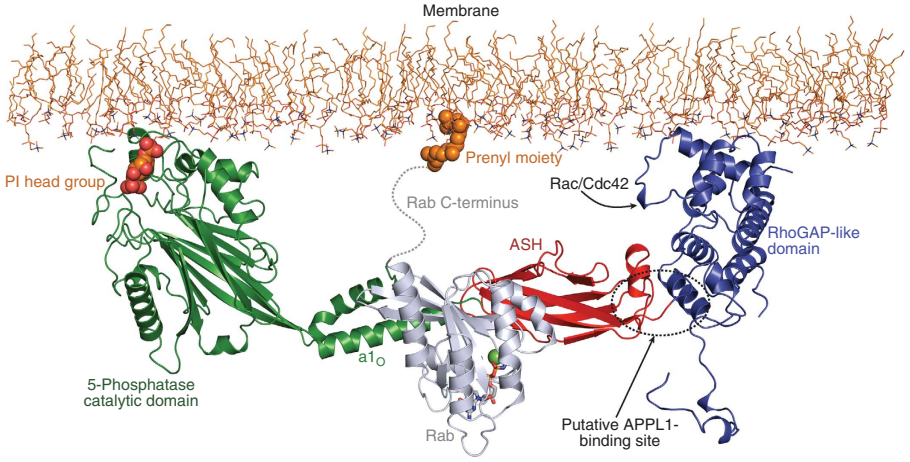

Figure 6 Structural model of the interaction of OCRL1 and Rab8a at the membrane interface. The inositol-5-phosphatase domain (Tsujishita *et al*, 2001) together with the ASH and RhoGAP-like domains (Erdmann *et al*, 2007) are docked at the membrane interface as reported previously. The N-terminal region of OCRL1 is not included. The Rab protein binds centrally between the 5-phosphatase and RhoGAP domains, with the nucleotide-binding pocket (sticks, GppNHp; green sphere, Mg^{2+}) facing towards the cytosol. In this model, binding of Rac/Cdc42 to the RhoGAP domain and APPL1 to OCRL1 (dashed circle) simultaneously with Rab8a is conceivable.

Figure 5 Structural and thermodynamic basis for the Lowe syndrome causing mutation F668V. (**A**) The residue $F668_O$ (red spheres) of the $\beta9_O$-strand of OCRL1 (red cartoon) is binding within a hydrophobic pocket of Rab8a (surface representation) located between Switch I and Switch II (the nucleotide is shown as ball and stick representation). (**B**) $F668_O$ is penetrating into a hydrophobic pocket of seven hydrophobic residues ($I41_R$, $G42_R$, $I43_R$, $A65_R$, $F70_R$, $I73_R$ and $Y77_R$). (**C**) Fluorescence polarization based equilibrium titrations of Rab8a:mantGppNHp with different $OCRL1_{539–901}$ variants (wild type, $F668V_O$ and $F668A_O$), demonstrating the significance of the Lowe disease related mutant $F668_O$ for Rab binding. The mutations $F668V_O$ and $F668A_O$ of OCRL1 decrease the affinity to Rab8a ($K_{D,Rab8:OCRL1\ wt} = 0.9\,\mu M$, $K_{D,Rab8:OCRL1\ F668V} = 5.2\,\mu M$, $K_{D,Rab8:OCRL1\ F668A} = 6.0\,\mu M$). (**D**) Pull-down experiment of Rab8a with GST–OCRL1 fusion proteins. Indicated GST-fusion proteins were incubated with Hela cell lysate, bound proteins were separated by SDS–polyacrylamide gel electrophoresis transferred to nitrocellulose and detected using anti-Rab8a or anti-APPL1 antibody, equal loading of GST-fusion proteins is indicated by ponceau staining. (**E**) Subcellular localization of OCRL1 F668V. Hela cells expressing GFP-tagged full-length OCRL1 or OCRL1 point mutant F668V were analysed by immunofluorescence microscopy with antibodies to the Golgi 58K protein. Insets show an enlargement of the Golgi area. (**F**) Comparison of subcellular localizations of OCRL1 wt with OCRL1 F668V. Hela cells were co-transfected with constructs for EGFP–OCRL1 F668V and Myc-tagged wild-type OCRL1 and analysed using immunofluorescence microscopy with antibodies against the Myc epitope (Bar, 10 μm).

pH 8.0, 500 mM NaCl, 2 mM β-mercaptoethanol) and eluted with a linear imidazole gradient (0–500 mM imidazole). Fractions containing the desired proteins were pooled, and the His_6-MBP-tag of OCRL1 was cleaved off overnight at 4°C with TEV protease or PreScission protease, respectively. Uncleaved protein, His_6-MBP and protease were removed via a Ni-NTA column, and the sample further purified by gel filtration over Superdex 75 column (GE Healthcare) pre-equilibrated with buffer containing 20 mM HEPES, pH 7.5, 100 mM NaCl and 2 mM dithioerythritol (DTE). Fractions containing OCRL1 fragments were pooled and concentrated. The $Rab8a_{6-176}$:GppNHp:$OCRL1_{540-678}$ complex was formed with 1.5-fold molar excess of $Rab8a_{6-176}$, purified via a Superdex 75 16/60 column (GE Healthcare), and concentrated $Rab8a_{6-176}$:GppNHp:$OCRL1_{540-678}$ to 17 mg/ml.

Crystallization and structure determination

The crystallization screening of the $Rab8a_{6-176}$:GppNHp:$OCRL1_{540-678}$ complex was carried out with the JCSG Core I-IV (Qiagen), using the sitting-drop vapour diffusion method at 20°C. Diffraction-quality crystals of the complex were grown against a reservoir solution containing 20% (w/v) polyethylene glycol 4000, 20% (v/v) glycerol, 0.16 M ammonium sulphate and 0.1 M sodium acetate at pH 4.6 by the hanging-drop vapour diffusion method. Diffraction data were collected at beamline X10SA of the Swiss Light Source and processed with XDS for indexing and data reduction (Kabsch, 1993). The structure of the complex was solved by molecular replacement in Phaser (McCoy *et al*, 2007) with poly-alanine derived from the coordinates of the Rab5:GppNHp (PDB entry code 1R2Q (Terzyan *et al*, 2004)) and the partial structure of OCRL1 (PDB entry code 2QV2 (Erdmann *et al*, 2007)) as search models. The initial crystallographic model was improved with iterative cycles of manual building in Coot (Emsley *et al*, 2010) and refinement in Refmac5 (Murshudov *et al*, 1997). Data collection and refinement statistics are shown in Table II. Structural figures were prepared with the program PyMol (Delano, 2002).

Preparative nucleotide exchange

Rab GTPases were incubated with a 20-fold molar excess of guanine nucleotides (mantGppNHp or GppNHp) and five-fold molar excess of EDTA over $MgCl_2$ for 2 h at 4°C. Unbound nucleotides were removed by NAP5 column (GE Healthcare) with the elution buffer consisting of 20 mM HEPES (pH 7.5), 50 mM NaCl, 1 mM $MgCl_2$, 2 mM DTE, 10 μM nucleotide. The efficiency of nucleotide exchange was determined by the reversed phase HPLC using a C-18 column under isocratic conditions (running buffer 50 mM potassium phosphate (pH 6.6), 10 mM tributylammonium bromide, and 8 or 25% (V/V) acetonitrile for GppNHp or mantGppNHp, respectively).

Fluorescence measurements

All fluorescence measurements were carried out at 25°C in buffer containing 50 mM HEPES (pH 7.5), 50 mM NaCl, 5 mM $MgCl_2$ and 5 mM DTE. Fluorescence equilibrium titrations were performed with a Fluoromax-3 fluorescence spectrometer (Horiba Jobin Yvon). The binding of OCRL1 to mantGppNHp-loaded Rabs was monitored by the change in fluorescence polarization (excitation 365 nm, emission 440 nm). The association and dissociation kinetics of Rab loaded with mantGppNHp were measured with a stopped-flow apparatus (Applied Photophysics) using the fluorescence polarization change (excitation at 365 nm, emission with a 420-nm cutoff filter). To monitor the influence of the APPL1/Ses1 peptides on Rab8a:mantGppNHp:OCRL1 affinity, the K_D of Rab8a:mantGppNHp with OCRL1 was determined as described above in the presence of 200 μM APPL1 peptide (sequence: SFQQRHESLRP) or 100 μM Ses1 peptide (sequence: PFARLHECYGQEI), respectively.

Analysis of fluorescence titrations

The concentration-dependent change in fluorescence polarization upon interaction of OCRL1 with Rab:mantGppNHp was fitted to a quadratic equation describing the binding isotherm of a reaction $R + O = RO$ (*R*: Rab, *O*: OCRL1, *RO*: Rab:OCRL1 complex). The titration can be described by the following equation

$$P = P_0 + \frac{P_\infty - P_0}{2 \cdot R_T} \cdot [(K_D + O_T + R_T) - \sqrt{(K_D + O_T + R_T)^2 - 4 \cdot O_T \cdot R_T}].$$

K_D is the equilibrium dissociation constant, O_T is the total (free and bound) concentration of OCRL1 at each titration step, R_T is the total (free and bound) concentration of Rab:mantGppNHp in the cuvette, P is the fluorescence polarization. P_0 and P_∞ are the fluorescence polarization values at $O_T = 0$ and $O_T = \infty$, respectively.

Immunofluorescence microscopy

Hela cells were plated on glass coverslips and transfected with the indicated expression constructs using Fugene 6 transfection reagent. At 48 h after transfection, cells were fixed with 4% paraformaldehyde, permeabilized with 0.5% Triton X-100 for 15 min at RT and blocked with 2% BSA for 30 min at RT. Cells were incubated with the following antibodies for 1 h at RT: mouse anti-Golgi 58K protein (Sigma-Aldrich, 1:100) or rabbit anti-c-myc (Santa Cruz, 1:40). After three washes with PBS, secondary Alexa Fluor 555-conjugated antibody (Molecular Probes, 1:400) was used for 1 h at RT. Cells were mounted on glass slides with Vectashield Mounting Medium (Axxora) and fluorescence was visualized with an Olympus inverted microscope.

Pull-down experiments and immunoblotting

Hela cells were lysed in lysis buffer (1 × PBS, 0.5% Triton X-100, protease inhibitors) and the cleared lysate was incubated with equal amounts of GST-fusion proteins bound to Glutathione Sepharose 4B (GE Healthcare) for 3 h at 4°C. After three washing steps with lysis buffer, bound proteins were eluted in 2 × Laemmli buffer for 10 min at 95°C and separated by SDS–polyacrylamide gel electrophoresis (SDS–PAGE). Proteins were transferred to nitrocellulose and incubated with mouse anti-Rab8a antibody (BD Biosciences, 1:1000) or goat anti-APPL1 antibody (Abcam, 1:2000) overnight at 4°C, followed by incubation with appropriate secondary HRP-conjugated antibodies. The blot was developed using the chemiluminescent Super Signal West Pico Chemilumiscent Substrate (Pierce).

Supplementary data

Supplementary data are available at *The EMBO Journal* Online (http://www.embojournal.org).

Acknowledgements

We thank N Bleimling for invaluable technical assistance, the staff of Beamline X10SA at the Paul Scherrer Institute (Villingen, Switzerland), and the X-ray communities at the Max-Planck-Institute (MPI) Dortmund and the MPI Heidelberg (Germany). Sascha Gentz and Florian Seebeck are acknowledged for the APPL1 and Ses1 peptide synthesis. The Dortmund Protein Facility is acknowledged for assistance in cloning and protein expression/purification. This work was supported by a Grant from the Deutsche Forschungsgemeinschaft SFB642, projects A4 and A17 to RSG and KSE, respectively.

Author contributions: XH determined the Rab8:OCRL1 complex crystal structure, performed the kinetics and wrote the paper. NH performed immunofluorescence, GST pull downs and immune blot analysis. SS analysed OCRL1 truncations. WB supervised the crystallographic analysis. RSG wrote the manuscript. KSE and AI designed the experiments and wrote the manuscript. Structural coordinates have been deposited in the PDB with the accession code 3QBT.

Conflict of interest

The authors declare that they have no conflict of interest.

References

Attree O, Olivos IM, Okabe I, Bailey LC, Nelson DL, Lewis RA, McInnes RR, Nussbaum RL (1992) The Lowe Oculocerebrorenal Syndrome Gene Encodes a Protein Highly Homologous to Inositol Polyphosphate-5-Phosphatase. *Nature* **358:** 239–242

Berrow NS, Alderton D, Sainsbury S, Nettleship J, Assenberg R, Rahman N, Stuart DI, Owens RJ (2007) A versatile ligation-independent cloning method suitable for high-throughput expression screening applications. *Nucleic Acids Res* **35:** e45

Bleimling N, Alexandrov K, Goody R, Itzen A (2009) Chaperone-assisted production of active human Rab8A GTPase in *Escherichia coli*. *Protein Expr Purif* **65:** 190–195

Burguete AS, Fenn TD, Brunger AT, Pfeffer SR (2008) Rab and Arl GTPase family members cooperate in the localization of the golgin GCC185. *Cell* **132:** 286–298

Chavas LM, Ihara K, Kawasaki M, Torii S, Uejima T, Kato R, Izumi T, Wakatsuki S (2008) Elucidation of Rab27 recruitment by its effectors: structure of Rab27a bound to Exophilin4/Slp2-a. *Structure* **16:** 1468–1477

Choudhury R, Diao A, Zhang F, Eisenberg E, Saint-Pol A, Williams C, Konstantakopoulos A, Lucocq J, Johannes L, Rabouille C, Greene LE, Lowe M (2005) Lowe syndrome protein OCRL1 interacts with clathrin and regulates protein trafficking between endosomes and the trans-Golgi network. *Mol Biol Cell* **16:** 3467–3479

Choudhury R, Noakes CJ, McKenzie E, Kox C, Lowe M (2009) Differential clathrin binding and subcellular localization of OCRL1 splice isoforms. *J Biol Chem* **284:** 9965–9973

Coon BG, Mukherjee D, Hanna CB, Riese DJ, Lowe M, Aguilar RC (2009) Lowe syndrome patient fibroblasts display Ocrl1-specific cell migration defects that cannot be rescued by the homologous Inpp5b phosphatase. *Hum Mol Genet* **18:** 4478–4491

Delano WL (2002) *The PyMOL Molecular Graphics System*, Version 1.3, Schrödinger, LLC

Delleman JW, Bleeker-Wagemakers EM, van Veelen AW (1977) Opacities of the lens indicating carrier status in the oculo-cerebro-renal (Lowe) syndrome. *J Pediatr Ophthalmol* **14:** 205–212

Di Paolo G, De Camilli P (2006) Phosphoinositides in cell regulation and membrane dynamics. *Nature* **443:** 651–657

Eathiraj S, Mishra A, Prekeris R, Lambright DG (2006) Structural basis for Rab11-mediated recruitment of FIP3 to recycling endosomes. *J Mol Biol* **364:** 121–135

Eathiraj S, Pan X, Ritacco C, Lambright DG (2005) Structural basis of family-wide Rab GTPase recognition by rabenosyn-5. *Nature* **436:** 415–419

Emsley P, Lohkamp B, Scott WG, Cowtan K (2010) Features and development of Coot. *Acta Crystallogr D Biol Crystallogr* **66:** 486–501

Erdmann KS, Mao Y, McCrea HJ, Zoncu R, Lee S, Paradise S, Modregger J, Biemesderfer D, Toomre D, De Camilli P (2007) A role of the Lowe syndrome protein OCRL in early steps of the endocytic pathway. *Dev Cell* **13:** 377–390

Faucherre A, Desbois P, Satre V, Lunardi J, Dorseuil O, Gacon G (2003) Lowe syndrome protein OCRL1 interacts with Rac GTPase in the trans-Golgi network. *Hum Mol Genet* **12:** 2449–2456

Fukuda M, Kanno E, Ishibashi K, Itoh T (2008) Large scale screening for novel Rab effectors reveals unexpected broad Rab binding specificity. *Mol Cell Proteomics* **7:** 1031–1042

Grosshans BL, Ortiz D, Novick P (2006) Rabs and their effectors: achieving specificity in membrane traffic. *Proc Natl Acad Sci USA* **103:** 11821–11827

Hichri H, Rendu J, Monnier N, Coutton C, Dorseuil O, Poussou RV, Baujat G, Blanchard A, Nobili F, Ranchin B, Remesy M, Salomon R, Satre V, Lunardi J (2010) From Lowe syndrome to Dent disease: correlations between mutations of the OCRL1 gene and clinical and biochemical phenotypes. *Hum Mutat* (doi:10.1002/humu.21391)

Hoopes Jr RR, Shrimpton AE, Knohl SJ, Hueber P, Hoppe B, Matyus J, Simckes A, Tasic V, Toenshoff B, Suchy SF, Nussbaum RL, Scheinman SJ (2005) Dent disease with mutations in OCRL1. *Am J Hum Genet* **76:** 260–267

Hyvola N, Diao A, McKenzie E, Skippen A, Cockcroft S, Lowe M (2006) Membrane targeting and activation of the Lowe syndrome protein OCRL1 by rab GTPases. *EMBO J* **25:** 3750–3761

Itzen A, Goody RS (2011) GTPases involved in vesicular trafficking: structures and mechanisms. *Semin Cell Dev Biol* **22:** 48–56

Jagoe WN, Lindsay AJ, Read RJ, Mccoy AJ, McCaffrey MW, Khan AR (2006) Crystal structure of Rab11 in complex with Rab11 family interacting protein 2. *Structure* **14:** 1273–1283

Janne PA, Suchy SF, Bernard D, MacDonald M, Crawley J, Grinberg A, Wynshaw-Boris A, Westphal H, Nussbaum RL (1998) Functional overlap between murine Inpp5b and Ocrl1 may explain why deficiency of the murine ortholog for OCRL1 does not cause Lowe syndrome in mice. *J Clin Invest* **101:** 2042–2053

Jefferson AB, Majerus PW (1995) Properties of type-Ii inositol polyphosphate 5-phosphatase. *J Biol Chem* **270:** 9370–9377

Joberty G, Tavitian A, Zahraoui A (1993) Isoprenylation of Rab proteins possessing a C-terminal Caax Motif. *FEBS Lett* **330:** 323–328

Kabsch W (1993) Automatic processing of rotation diffraction data from crystals of initially unknown symmetry and cell constants. *J Appl Crystallogr* **26:** 795–800

Kawasaki M, Nakayama K, Wakatsuki S (2005) Membrane recruitment of effector proteins by Arf and Rab GTPases. *Curr Opin Struct Biol* **15:** 681–689

Kenworthy L, Charnas L (1995) Evidence for a discrete behavioral phenotype in the oculocerebrorenal syndrome of Lowe. *Am J Med Genet* **59:** 283–290

Kleta R (2008) Fanconi or not Fanconi? Lowe syndrome revisited. *Clin J Am Soc Nephrol* **3:** 1244–1245

Kukimoto-Niino M, Sakamoto A, Kanno E, Hanawa-Suetsugu K, Terada T, Shirouzu M, Fukuda M, Yokoyama S (2008) Structural basis for the exclusive specificity of Slac2-a/melanophilin for the Rab27 GTPases. *Structure* **16:** 1478–1490

Lee MTG, Mishra A, Lambright DG (2009) Structural mechanisms for regulation of membrane traffic by Rab GTPases. *Traffic* **10:** 1377–1389

Lowe M (2005) Structure and function of the Lowe syndrome protein OCRL1. *Traffic* **6:** 711–719

Mao YX, Balkin DM, Zoncu R, Erdmann KS, Tomasini L, Hu FH, Jin MM, Hodsdon ME, De Camilli P (2009) A PH domain within OCRL bridges clathrin-mediated membrane trafficking to phosphoinositide metabolism. *EMBO J* **28:** 1831–1842

McCoy AJ, Grosse-Kunstleve RW, Adams PD, Winn MD, Storoni LC, Read RJ (2007) Phaser crystallographic software. *J Appl Crystallogr* **40:** 658–674

Mellman I, Nelson WJ (2008) Coordinated protein sorting, targeting and distribution in polarized cells. *Nat Rev Mol Cell Biol* **9:** 833–845

Merithew E, Hatherly S, Dumas JJ, Lawe DC, Heller-Harrison R, Lambright DG (2001) Structural plasticity of an invariant hydrophobic triad in the switch regions of Rab GTPases is a determinant of effector recognition. *J Biol Chem* **276:** 13982–13988

Mishra A, Eathiraj S, Corvera S, Lambright DG (2010) Structural basis for Rab GTPase recognition and endosome tethering by the C2H2 zinc finger of early endosomal autoantigen 1 (EEA1). *Proc Natl Acad Sci USA* **107:** 10866–10871

Moorhead AM, Jung JY, Smirnov A, Kaufer S, Scidmore MA (2010) Multiple host proteins that function in phosphatidylinositol-4-phosphate metabolism are recruited to the chlamydial inclusion. *Infect Immun* **78:** 1990–2007

Murshudov GN, Vagin AA, Dodson EJ (1997) Refinement of macromolecular structures by the maximum-likelihood method. *Acta Crystallogr D Biol Crystallogr* **53:** 240–255

Ooms LM, Horan KA, Rahman P, Seaton G, Gurung R, Kethesparan DS, Mitchell CA (2009) The role of the inositol polyphosphate 5-phosphatases in cellular function and human disease. *Biochem J* **419:** 29–49

Ostermeier C, Brunger AT (1999) Structural basis of Rab effector specificity: crystal structure of the small G protein Rab3A complexed with the effector domain of rabphilin-3A. *Cell* **96:** 363–374

Recacha R, Boulet A, Jollivet F, Monier S, Houdusse A, Goud B, Khan AR (2009) Structural basis for recruitment of Rab6-interacting protein 1 to Golgi via a RUN domain. *Structure* **17:** 21–30

Rodriguez-Gabin AG, Ortiz E, Demoliner K, Si Q, Almazan G, Larocca JN (2010) Interaction of Rab31 and OCRL-1 in oligodendrocytes: its role in transport of Mannose 6-phosphate receptors. *J Neurosci Res* **88:** 589–604

Segev N (2001) Ypt/Rab GTPases: regulators of protein trafficking. *Sci STKE* **2001:** re11

Shrimpton AE, Hoopes Jr RR, Knohl SJ, Hueber P, Reed AA, Christie PT, Igarashi T, Lee P, Lehman A, White C, Milford DV, Sanchez MR, Unwin R, Wrong OM, Thakker RV, Scheinman SJ (2009) OCRL1 mutations in Dent 2 patients suggest a mechanism for phenotypic variability. *Nephron Physiol* **112:** p27–p36

Stenmark H (2009) Rab GTPases as coordinators of vesicle traffic. *Nat Rev Mol Cell Biol* **10:** 513–525

Swan LE, Tomasini L, Pirruccello M, Lunardi J, De Camilli P (2010) Two closely related endocytic proteins that share a common OCRL-binding motif with APPL1. *Proc Natl Acad Sci USA* **107:** 3511–3516

Terzyan S, Zhu GY, Li GP, Zhang XJC (2004) Refinement of the structure of human Rab5a GTPase domain at 1.05 angstrom resolution. *Acta Crystallogr D Biol Crystallogr* **60:** 54–60

Tsujishita Y, Guo SL, Stolz LE, York JD, Hurley JH (2001) Specificity determinants in phosphoinositide dephosphorylation: Crystal structure of an archetypal inositol polyphosphate 5-phosphatase. *Cell* **105:** 379–389

Ungewickell A, Ward ME, Ungewickell E, Majerus PW (2004) The inositol polyphosphate 5-phosphatase Ocrl associates with endosomes that are partially coated with clathrin. *Proc Natl Acad Sci USA* **101:** 13501–13506

Utsch B, Bokenkamp A, Benz MR, Besbas N, Dotsch J, Franke I, Frund S, Gok F, Hoppe B, Karle S, Kuwertz-Bröking E, Laube G, Neb M, Nuutinen M, Ozaltin F, Rascher W, Ring T, Tasic V, van Wijk JA, Ludwig M (2006) Novel OCRL1 mutations in patients with the phenotype of Dent disease. *Am J Kidney Dis* **48:** 942.e1–942.e14

Wu M, Wang T, Loh E, Hong W, Song H (2005) Structural basis for recruitment of RILP by small GTPase Rab7. *EMBO J* **24:** 1491–1501

Zhu GY, Zhai P, Liu J, Terzyan S, Li GP, Zhang XJC (2004) Structural basis of Rab5-Rabaptin5 interaction in endocytosis. *Nat Struct Mol Biol* **11:** 975–983

